

Heuristic Rank Selection with Progressively Searching Tensor Ring Network

Nannan Li^{1, 2*}, Yu Pan^{3*}, Yaran Chen^{1, 2}, Zixiang Ding^{1, 2}, Dongbin Zhao^{1, 2}, Zenglin Xu^{4, 5}

¹ The State Key Laboratory of Management and Control for Complex Systems, Institute of Automation, Chinese Academy of Sciences, Beijing, China

² University of Chinese Academy of Sciences, Beijing, China

³ University of Electronic Science and Technology of China, Chengdu, China

⁴ Pengcheng Lab, Shenzhen, China

⁵ Harbin Institute of Technology (Shenzhen), Shenzhen, China

Abstract

Recently, Tensor Ring Networks (TRNs) have been applied in deep networks, achieving remarkable successes in compression ratio and accuracy. Although highly related to the performance of TRNs, rank is seldom studied in previous works and usually set to equal in experiments. Meanwhile, there is not any heuristic method to choose the rank, and an enumerating way to find appropriate rank is extremely time-consuming. Interestingly, we discover that part of the rank elements is sensitive and usually aggregate in a certain region, namely an interest region. Therefore, based on the above phenomenon, we propose a novel progressive genetic algorithm named Progressively Searching Tensor Ring Network Search (PSTRN), which has the ability to find optimal rank precisely and efficiently. Through the evolutionary phase and progressive phase, PSTRN can converge to the interest region quickly and harvest good performance. Experimental results show that PSTRN can significantly reduce the complexity of seeking rank, compared with the enumerating method. Furthermore, our method is validated on public benchmarks like MNIST, CIFAR10/100 and HMDB51, achieving the state-of-the-art performance.

1 Introduction

Deep neural networks have made great successes in various areas, such as image classification (He et al. 2016; Simonyan and Zisserman 2015), autonomous driving (Chen et al. 2018; Zhao et al. 2017; Li et al. 2018), game artificial intelligence (Shao et al. 2018; Li et al. 2019) and so on. However, parameters redundancy leads to two major drawbacks for deep neural networks: 1) difficult training, and 2) poor ability to run on resource-constrained devices (e.g., mobile phones (Kim et al. 2016) and Internet of Things (IoT) devices (Lane et al. 2015)). To address these problems, Tensor Ring (TR) has been introduced to deep neural networks. With a ring-like structure as shown in Figure 2, TR can significantly reduce the parameters of Convolutional Neural Network (CNN) (Wang et al. 2018) and Recurrent Neural Network (RNN) (Pan et al. 2019), and even can achieve better results than uncompressed models in some tasks. Thus tensor ring is increasingly being researched.

However, as the crucial component of tensor ring, setting of rank (e.g. $R_0 \sim R_3$ in Figure 2) is seldom investigated. In most of the existing works, it merely sets to be equal in whole network (Wang et al. 2018). Such an equal setting requires multiple manual attempts for a feasible rank value and often leads to a weak result. Fortunately, as shown in our synthetic experiment, we discover the relationship between the rank distribution and its performance. Experimental results demonstrate the link that part of rank elements with good performance will gather to the interest region. Then we extend this phenomenon to build our Hypothesis 1. Utilizing the hypothesis, we design a heuristic algorithm to explore the potential power of tensor ring.

Specifically, we propose Progressive Searching Tensor Ring Network (PSTRN) inspired by Neural Architecture Search (NAS) (Zoph and Le 2017). Similarly, our approach is divided into three parts,

- search space: combinations of rank element candidates for TRN in evolutionary phase;
- search strategy: the Non-dominated Sorted Genetic Algorithm-II (NSGA-II) (Deb et al. 2002) to search rank;
- performance estimation strategy: stochastic gradient descent to train TRN.

The overall framework of PSTRN is illustrated in Figure 1. In the searching process, we initialize search space first. Then through evolutionary phase, we derive optimized rank within search space. Next, in order to draw near interest region, the proposed approach shrinks the bound of search space to the around of optimized rank during progressive phase. By alternately executing evolutionary phase and progressive phase, our algorithm can find rank with high performance. Additionally, on large-scale models (i.e. ResNet20 and ResNet32 (He et al. 2016)), the performance estimation is time-consuming, which is harmful to search speed. So we employ a weight inheritance strategy (Real et al. 2017) to accelerate the evaluation of rank.

Experimental results prove that PSTRN can obtain optimal rank of TRN according to the Hypothesis 1. And our algorithm can compress LeNet-5 (LeCun et al. 1998) with compression ratio as 16x and 0.49% error rate in MNIST (Deng 2012) image classification task. In TR-ResNets, our approach can achieve state-of-the-art performance on CIFAR10 and CIFAR100 (Krizhevsky, Hinton et al. 2009).

@ Preprint.

*These authors contributed equally to this work.

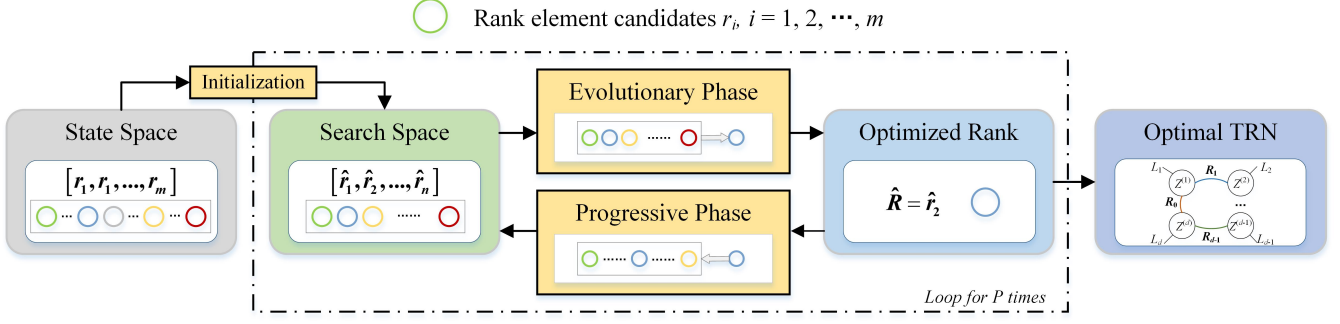


Figure 1: The overview of Progressive Searching Tensor Ring Network (PSTRN), where different color represents different rank element candidate. PSTRN initializes search space by sampling from state space, then alternately executes evolutionary phase and progressive phase for P times to derive optimal TRN.

PSTRN also exceeds TR-LSTM models that set rank elements equal on HMDB51. Furthermore, compared with the enumerating method, our work can greatly reduce the complexity of seeking rank. Overall, our contributions can be summarized as follows:

1. PSTRN can search rank automatically instead of manual setting. At the meantime, The time cost is reduced significantly by progressively searching, compared with an enumerating method.
2. To speed up the search on large-scale model, our proposed method adopts weight inheritance into the search process. And the proposed method achieves about $200\times$ speed-up ratio on classification tasks of CIFAR10/100 datasets .
3. As a heuristic approach based on the Hypothesis 1, our algorithm can achieve better performance with fewer parameters than existing works. All the experimental results demonstrate the rationality of the Hypothesis that is first found by us.

2 Background

In this section, we will introduce the tensor ring format and some related works that consist of rank fixed method and rank selection method. The rank fixed method is the work that sets rank manually, while rank selection method means the work of learning the rank. Besides, some notations and operations are listed in the Supplementary Material.

2.1 Tensor Ring Format (TRF)

TRF is constructed with a series of 3-order nodes linked one by one, forming a ring-like structure. The TRF of a d -order tensor can be formulated as

$$\mathcal{T}_{l_1, l_2, \dots, l_d} = \sum_{R_0, R_1, \dots, R_{d-1}} \mathcal{Z}_{r_0, l_1, r_1}^{(1)} \mathcal{Z}_{r_1, l_2, r_2}^{(2)} \dots \mathcal{Z}_{r_{d-1}, l_d, r_0}^{(d)}, \quad (1)$$

where $\mathbf{R} = \{R_i | i \in \{0, 1, \dots, d-1\}\}$ denotes the rank of TRF, and the symbol \mathcal{Z} represents the tensor ring node. Figure 2 shows a graph structure of a simple TRF. Through replacing layers(e.g. convolutional layer, fully-connected layer) of a network with TRF, we can derive a TRN.

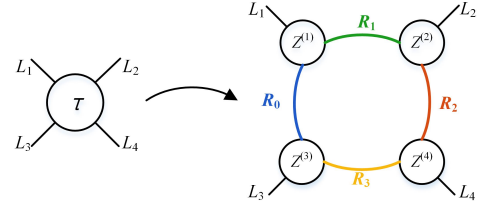


Figure 2: The representations of TRF.

2.2 Rank Fixed

Tensor ring decomposition has been successfully applied to the compression of deep neural networks. Wang et al. (2018) compresses both the fully connected layers and the convolutional layers of CNN with the equal rank elements for whole network. Pan et al. (2019) replaces the over-parametric input-to-hidden layer of LSTM with TRF, when dealing with high-dimensional input data. Rank of these models are determined via multiple manual attempts by manipulation, which requires much time.

2.3 Rank Selection

In this part, we would like to introduce the works of rank selection. Yerlan and Miguel (2020) formulate the low-rank compression problem as a mixed discrete-continuous optimization jointly over the rank elements and over the matrix elements. Cheng et al. (2020) propose a novel rank selection scheme for tensor ring, which apply deep deterministic policy gradient to control the selection of rank. Their algorithms calculate the optimal rank directly from the trained weight matrix without the analysis of rank. Different from them, our approach is inspired by the relevance between the rank distribution and performance of Hypothesis 1, towards a better result.

3 Methodology

To verify the optimization of PSTRN on TRN, we choose two most commonly used deep neural networks for evaluation, i.e. Tensor Ring CNN (TR-CNN) and Tensor Ring LSTM (TR-LSTM).

In the section, we first present preliminaries of TR-CNN and TR-LSTM, including graphical illustrations of the two TR-based models. Then we elaborate on evolutionary phase and progressive phase of PSTRN. The implementation of weight inheritance will be given in final.

3.1 Preliminaries

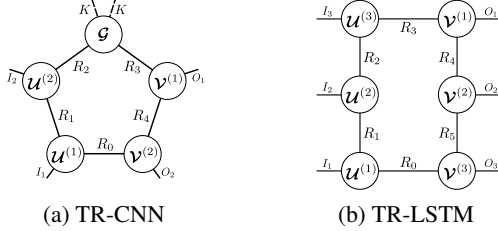


Figure 3: Tensor Ring Model

TR-CNN For a convolutional core $\mathcal{C} \in \mathbb{R}^{K \times K \times C_{in} \times C_{out}}$ where K denotes the kernel size, C_{in} means the input channel and C_{out} represents the output channel. We first reshape it as $\hat{\mathcal{C}} \in \mathbb{R}^{K \times K \times I_1 \times \dots \times I_\alpha \times O_1 \times \dots \times O_\beta}$, satisfying the rule

$$C_{in} = \prod_{i=1}^{\alpha} I_i, \quad C_{out} = \prod_{j=1}^{\beta} O_j. \quad (2)$$

Then we decompose it into input nodes $\mathcal{U}^{(i)} \in \mathbb{R}^{R_{i-1} \times I_i \times R_i}, i \in \{1, 2, \dots, \alpha\}$, output nodes $\mathcal{V}^{(j)} \in \mathbb{R}^{R_{\alpha+j} \times O_j \times R_{\alpha+j+1}}, j \in \{1, 2, \dots, \beta\}$ and one convolutional node $\mathcal{G} \in \mathbb{R}^{K \times K \times R_\alpha \times R_{\alpha+1}}$, where $R_{\alpha+\beta+1} = R_0$. An instance ($\alpha = 2, \beta = 2$) is illustrated in Figure 3a. And the compression ratio of TR-CNN is calculated as

$$C_{CNN} = \frac{K^2 C_{in} C_{out}}{\sum_{i=1}^{\alpha} R^2 I_i + \sum_{j=1}^{\beta} R^2 O_j + K^2 R^2}, \quad (3)$$

where R is a simplification of rank element. The calculation of the TR-CNN could be found in Wang et al. (2018).

TR-LSTM By replacing each matrix of the affine matrices $\mathbf{W}_* \in \mathbb{R}^{I \times O}$ of input vector $x \in \mathbb{R}^I$ with TRF in LSTM, we implement the TR-LSTM model as introduced in Pan et al. (2019). Similar to TR-CNN, the nodes are combined by input nodes $\mathcal{U}^{(i)}$ and output nodes $\mathcal{V}^{(j)}$, and the decomposition needs to follow

$$I = \prod_{i=1}^{\alpha} I_i, \quad O = \prod_{j=1}^{\beta} O_j. \quad (4)$$

A 6-node example is shown in Figure 3b. Compression ratio of TR-LSTM can be computed as

$$C_{RNN} = \frac{IO}{\sum_{i=1}^{\alpha} R^2 I_i + \sum_{j=1}^{\beta} R^2 O_j}. \quad (5)$$

3.2 Progressive Searching Tensor Ring Network

In our search process, the rank \mathbf{R} of a TRN is formulated as

$$\mathbf{R} = \{R_0, R_1, \dots, R_{d-1} | R_* \in \{r_1, r_2, \dots, r_m\}\}, \quad (6)$$

where d is the number of rank elements, r_* is a rank element candidate, and m is the quantity of rank element candidates. Full combinations of the rank elements (i.e. state space) can be calculated as

$$S_{state} = m^d. \quad (7)$$

Next, we would like to introduce the Hypothesis 1, the extension of the aforementioned gathering phenomenon.

Hypothesis 1 When a shape-fixed TRN performs well, part or all of its rank elements are sensitive and each of them will tend to aggregate in a certain region, which is called interest region.

According to Hypothesis 1, the optimal rank can be found in the interest region. It is a more efficient and accurate way to find a optimal rank in interest region rather than a much wider range of the whole rank element candidates. Thus, we build an pipeline of PSTRN to achieve the purpose by two alternative procedures:

- Evolutionary phase: finding good models in the search space and locating the interest region through well-performed models.
- Progressive phase: calculating the width of a rough approximation of interest region and defining search space within this region.

Through these two procedures, the rank of a TRN will approach the interest region and be optimized. Additionally, we apply weight inheritance to accelerate the training process. The pseudocode of the algorithm is shown in Supplemental Material.

Evolutionary Phase As described in Hypothesis 1 that well-performed models aggregate in interest region, good models keep a high probability of appearing in interest region. Therefore, we determine interest region around the models with high performance.

In PSTRN, we adopt multi-objectives genetic algorithm NSGA-II (Deb et al. 2002) to search for TR-based models with high performance and few parameters.

A typical genetic algorithm requires two prerequisites, the genetic representation of solution domain (i.e. search space), and the fitness functions (i.e. classification accuracy and compression ratio) that is used to evaluate each individual. In the process, an individual means the rank \mathbf{R} and each rank element R_* is in $\{\hat{r}_1, \hat{r}_2, \dots, \hat{r}_n\}$ that is sampled from the whole rank element candidates. The search space is a sub-space of the state space and can be calculated as

$$S_{search} = n^d. \quad (8)$$

The method of choosing the search space will be introduced in the progressive phase. Classification accuracy is obtained by testing the model on the test dataset. And compression ratio of TR-CNN and TR-LSTM are calculated by Eq (3) and Eq (5) respectively.

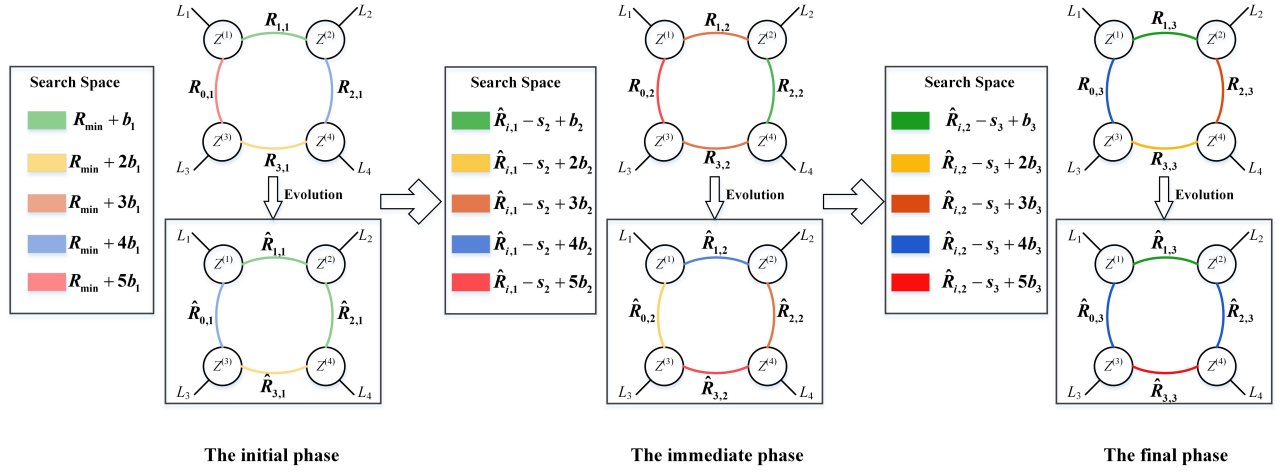


Figure 4: The overall pipeline of progressive phase, where different color represents different rank. The search space is sampled at interval b within given range first. Then we gradually reduce the interval b . Obviously, progressive phase narrows search space close to interest region progressively.

The key idea of the genetic algorithm is to evolve individuals via some genetic operations. At each evolutionary generation, the selection process preserves strong individuals as a population and then sorts them according to their fitness function, while eliminating weak ones. The retained strong individuals reproduce new children through mutation and crossover with a certain probability. After this, we obtain the new population consists of the new children and the retained strong individuals. The new population executes the evolution to derive next generation. When the termination condition is met, evolutionary phase stops and optimization of the rank will be completed. Eventually, taking the top- k individuals into consider, we derive the most promising rank element \hat{R}_* by

$$\hat{R}_* = \text{floor}\left(\frac{1}{k} \sum_{i=1}^k R_{*,i}\right), \quad (9)$$

where $R_{*,i}$ is a rank element of the i -th individual and floor denotes the rounding down operation. The interest region is around the \hat{R}_* .

Progressive Phase Progressive phase is used to determine the next search space as shown in Figure 4. At the beginning of the PSTRN, we first obtain initial search space via sampling from the state space at equal intervals as below:

$$\{R_{\min} + b_1, R_{\min} + 2b_1, \dots, R_{\min} + nb_1\}, \quad (10)$$

where R_{\min} is the minimum of rank element candidates, and b_1 is the initial sampling interval. Then through carrying out evolutionary phase within initial search space, we derive the promising rank

$$\hat{R} = \{\hat{R}_{0,1}, \hat{R}_{1,1}, \dots, \hat{R}_{d-1,1}\}, \quad (11)$$

where $\hat{R}_{i,j}, i \in \{0, 1, 2, \dots, d-1\}, j \in \{2, 3, \dots, P\}$ denotes the i -th promising rank element in j -th evolutionary phase. Based on the optimized rank, our PSTRN shrinks bound of search space to:

- Low Bound: $\min(\hat{R}_{i,j-1} - s_j, R_{\min})$,
- High Bound: $\max(\hat{R}_{i,j-1} + s_j, R_{\max})$,

where R_{\max} is the maximum of rank element candidates, and $\{s_j | j \in \{2, 3, \dots, P\}\}$ is the offset coefficient and usually sets to b_{j-1} . Thus the rank element candidates of the next search space can be expressed as:

$$\{\hat{R}_{i,j-1} - s_j + b_j, \hat{R}_{i,j-1} - s_j + 2b_j, \dots, \hat{R}_{i,j-1} - s_j + nb_j\}, \quad (12)$$

where b_j is the sampling interval of the j -th progressive phase, satisfying

$$b_{j+1} \leq b_j, j \in \{1, 2, \dots, P\}. \quad (13)$$

The interval b_j is gradually reduced, and when b_j decreases to 1, the progressive phase will stop.

In addition, considering the above Hypothesis 1 cannot be proved by theory, the progressive genetic algorithm may fall into local optima. Therefore, we adds an exploration mechanism to the algorithm. Concretely speaking, except for the initial phase, the algorithm has a 10% probability to choose rank within the search space in the previous evolutionary phase.

In the above evolutionary phase, the solution domain is one of the key components. Generally speaking, it will try to cover all possible states. Such an excessive solution domain may lead to the divergence of search algorithm. Compared with full state space, our algorithm can improve the search process in computational complexity significantly.

Weight Inheritance During evolutionary phase, to validate the performance, the searched TRN needs to be fully trained, which is the most time-consuming part of the search process. On MNIST, we can train searched TR-LeNet5 from scratch because of its fast convergence. But the training speed is slow on ResNets. Thus we employ weight inheritance as a performance estimation acceleration strategy,

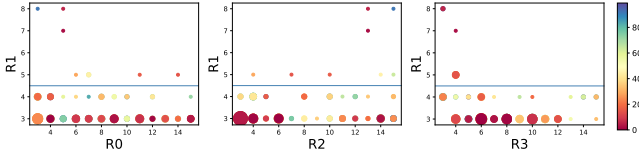


Figure 5: Rank distribution between R_1 and other rank elements R_0, R_2, R_3 of top-100 models. The size of the circle denotes the number of models that has the same two rank elements, and the circle color represents ranking. The blue line is the border of the interest region.

which is inspired by the architecture evolution (Real et al. 2017).

In our algorithm, to inherit trained weight directly, the rank $R = \{R_i^k | i \in [0, 1, \dots, d-1]\}$ of k -th layer needs to follow

$$R_0^k = R_1^k = \dots = R_{d-1}^k = V_k. \quad (14)$$

Obviously, the number of rank elements to be searched is reduced to k from d . For the k -th layer, we will load the checkpoint whenever possible. Namely, if the k -th layer matches V_k , the weights are preserved. Such a method is called warm-up.

During search process, we directly inherit the weights trained in warm-up stage and fine-tune the weights for each searched TRN. Instead of training from scratch, fine-tuning the trained weights can greatly resolve the time-consuming problem. For example, training ResNet20 on CIFAR10 from scratch requires about 200 epochs. On the contrary, our training with fine-tuning only needs 1 epoch, which brings the acceleration of $200\times$.

4 Experiments

In this section, we conduct experiments to verify the effectiveness of PSTRN. First, to display the relation between the rank elements and performance of TR-based models, we design the synthetic experiment. Then we estimate the effect of the searched TR-based models on prevalent benchmarks. The optimization objectives of NSGA-II (Deb et al. 2002) are classification performance and compression ratio, namely PSTRN-M. In addition, to gain the TR-based model with high performance, we also conduct optimization algorithm PSTRN-S that only consider classification accuracy. All the experiments are implemented on Nvidia Tesla V100 GPUs. In addition, some specific experimental settings and rank elements of optimal model are shown in Supplementary Material.

4.1 Synthetic Experiment

Previous works of rank search lack of heuristic method, so they derive rank elements depending on decomposition, which limits the exploration of searching rank. Hypothesis 1 would bring a promising way to solve this problem, and we would like show the phenomenon of interest region in a synthetic experiment.

Experimental Setting Given a low-rank weight matrix $\mathbf{W} \in \mathbb{R}^{144 \times 144}$. We generate 5000 samples, and each dimension follows the normal distribution, i.e. $x \sim \mathcal{N}(0, 0.05\mathbf{I})$, where $\mathbf{I} \in \mathbb{R}^{144}$ is the identity matrix. Then we generate the label y according to $y = \mathbf{W}(x + \epsilon)$ for each x , where $\epsilon \sim \mathcal{N}(0, 0.05\mathbf{I})$ is a random Gaussian noise. Data pairs of $\{x, y\}$ constitute the dataset. We divide it into 4000 samples as the training set and 1000 samples as the testing set. For the model, we constructed the TR-linear model by replacing the $\mathbf{W} \in \mathbb{R}^{144 \times 144}$ with a TRF $\in \mathbb{R}^{12 \times 12 \times 12 \times 12}$. Then we train the TR-linear model with different ranks to completion, and validate the performance on the testing set with Mean-Square Error (MSE) between the prediction \hat{y} and label y . The rank is denoted as $\mathbf{R} = \{R_0, R_1, R_2, R_3 | R_* \in \{3, 4, \dots, 15\}\}$.

In the experiment, optimizer sets to Adam with a learning rate $1e-2$, MSE is adopted as loss function and batch size is 128. The total epoch is 100, and the learning rate decreases 90% every 30 epoch. For a comparison, we run the enumerating results as the baseline, which needs $13^4 = 28561$ times training.

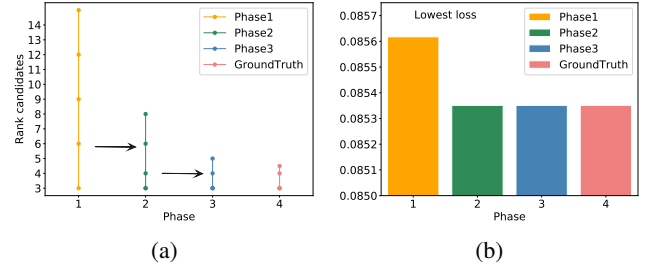


Figure 6: (a) Interest region approximation of three phases, and groundtruth is the interest region. (b) Rank performance of models. There are lowest losses of first phase, second phase, third phase and groundtruth from left to right sequentially.

Experimental Results Figure 5 shows the distribution of top-100 rank elements sorted by the value of loss. The size of the circle denotes the number of models who has the same two rank elements. And the circle color represents ranking. It shows that it is not ideal to set each rank element the same arbitrarily. We calculate the mean $\mu(3.6)$ and standard variance $\delta(0.96)$ of top-100 models, and derive the interest region $[\mu - \delta, \mu + \delta]([2.64, 4.56])$. Obviously, R_1 mostly distributes in the interest region. Should be noted that other rank elements do not show an apparent phenomenon, for the reason that they do not play a critical role in the performance. Our model can find the interest region that is important to the ability of models and achieve good results.

As shown in Figure 6a, the approximation of interest region gradually approaches groundtruth, which demonstrates that PSTRN can locate interest region precisely. As illustrated in Figure 6b, our model can find the best rank in the second phase, which proves the powerful capacity of PSTRN algorithm. Compared with 28561 enumerating results, we only need $n_{gen} \times pop_size \times P = 20 \times 10 \times 3 =$

600 times training, which is much smaller. And pop_size and n_gen are the population size and the number of generations respectively. Undoubtedly, our PSTRN can find the optimal rank efficiently and precisely.

4.2 Experiments on Mnist and Fashion MNIST

MNIST dataset has 60k grayscale images with 10 object classes, and the resolution of each data is 28×28 . Fashion MNIST is more complicated and easy to replace MNIST in experiments.

Experimental Setting We evaluate our PSTRN on MNIST and Fashion MNIST by searching TR-LeNet5 that is proposed in Wang et al. (2018). The TR-LeNet5 is constructed with two tensor ring convolutional layers and two tensor ring fully-connected layers. Thus, the total rank is $R = \{R_0, R_1, \dots, R_{19} | R_* \in \{2, 3, \dots, 30\}\}$. Accordingly, the computational complexity size is $29^{20} \approx 1.77 \times 10^{29}$ for enumeration, while complexity of our PSTRN is $n_gen \times pop_size \times P = 30 \times 40 \times 3 = 3600$.

Table 1: Comparison with state-of-the-art results for LeNet-5 on MNIST.

Model	Error(%)	Params(K)	CR
Original	0.79	429	1
TR-Nets($r = 10$)	1.39	11	$39 \times$
TR-Nets($r = 20$)	0.69	41	$11 \times$
TR-Nets($r = 30$) ^{ri}	0.70	145	$3 \times$
BAMC	0.83	-	-
LR-L	0.75	27	$15.9 \times$
PSTRN-M(Ours)	0.57	26	$16.5 \times$
PSTRN-S(Ours)	0.49	66	$6.5 \times$

Experimental Results Experimental results are summarized in Table 1, where original LeNet-5 is proposed in LeCun et al. (1998), Bayesian Automatic Model Compression(BAMC) (Wang et al. 2020) leverages Dirichlet process mixture models to explore the layer-wise quantization policy, LR-L (Yerlan and Miguel 2020) learn the rank of each layer for SVD, and TR-Nets (Wang et al. 2018) compresses deep neural network via tensor ring decomposition with equal rank elements. The superscript ^{ri} represents there are results of re-implement, and r is the rank of works that set rank elements to equal. These settings would be retained in subsequent experiments. In Table 1, the first block shows the results of rank-fixed methods, which manually set rank elements to equal. The second block is the work that automatically compresses the model. As expected, both PSTRN-M and PSTRN-S achieve best performance on MNIST. Our algorithm compress LeNet-5 with compression ratio as 6.5x and 0.49% error rate. For the results on Fashion MNIST, as shown Figure 7, our proposed approach outperforms rank-fixed works as well. Obviously, when fixed rank r is bigger than 20, the TRN will be over-fitting. And our proposed work can find the suitable rank with best performance.

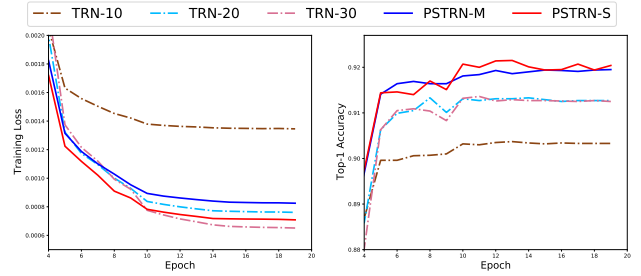


Figure 7: Training processes on Fashion MNIST.

Table 2: Comparison with state-of-the-art results for ResNet20 on CIFAR.

Model	Error(%)	Params(M)	CR
CIFAR10			
Original	8.75	0.27	1
TR-Nets($r = 10$)	12.5	0.05	$5.40 \times$
TR-RL	11.7	0.04	$6.75 \times$
LR-L	12.89	0.05	$5.40 \times$
PSTRN-M(Ours)	11.50	0.04	$6.75 \times$
LR-L	9.49	0.11	$2.45 \times$
TR-Nets($r = 15$) ^{ri}	9.22	0.12	$2.25 \times$
PSTRN-S(Ours)	9.20	0.11	$2.45 \times$
CIFAR100			
Original	34.60	0.28	1
TR-Nets($r = 10$) ^{ri}	36.45	0.06	$4.7 \times$
PSTRN-M(Ours)	36.38	0.06	$4.7 \times$
TR-Nets($r = 15$) ^{ri}	34.49	0.14	$2.0 \times$
PSTRN-S(Ours)	33.87	0.12	$2.3 \times$

4.3 Experiments on CIFAR10 and CIFAR100

Both CIFAR10 and CIFAR100 datasets consist of 50,000 train images and 10,000 test images with size as $32 \times 32 \times 3$. CIFAR10 has 10 object classes and CIFAR100 has 100 categories.

Experimental Setting TR-ResNet32 is built as introduced in Wang et al. (2018), and TR-ResNet20 is constructed as proposed in Cheng et al. (2020). First, we apply the PSTRN-M/S to search TR-ResNet20/32 on CIFAR10. Further, we transfer TR-ResNet20/32 searched by PSTRN-M/S on CIFAR10 into CIFAR100 to evaluate the transferability of PSTRN. Considering that training TR-ResNet20/32 on CIFAR10 is time-consuming, we apply the weight inheritance to accelerate the process. Specifically, we pre-train weight of the model in warm-up stage. Then we load pre-trained weights directly. The training epoch of warm-up is set to 30. The rank $R = \{R_0, R_1, \dots, R_7 | R_* \in \{2, 3, \dots, 20\}\}$. The complexity of our approach is $n_gen \times pop_size \times P = 30 \times 40 \times 3 = 3600$, which is much smaller than computational complexity $19^7 \approx 8.9 \times 10^8$ of enumeration method.

Table 3: Comparison with state-of-the-art results for ResNet32 on CIFAR.

Model	Error(%)	Params(M)	CR
CIFAR10			
Original	7.5	0.46	1
Tucker	12.3	0.09	$5.1 \times$
TT($r = 13$)	11.7	0.10	$4.8 \times$
TR-Nets($r = 10$)	9.4	0.09	$5.1 \times$
TR-RL	11.9	0.03	$1.5 \times$
LR-L	10.56	0.09	$5.1 \times$
PSTRN-M(Ours)	9.4	0.08	$5.8 \times$
TR-Nets($r = 15$) ^{<i>ri</i>}	8.76	0.20	$2.3 \times$
PSTRN-S(Ours)	8.56	0.17	$2.7 \times$
CIFAR100			
Original	31.90	0.47	1
Tucker	42.20	0.09	$5.1 \times$
TT($r = 13$)	37.10	0.10	$4.6 \times$
TR-Nets($r = 10$)	33.30	0.097	$4.8 \times$
PSTRN-M(Ours)	33.23	0.091	$5.2 \times$
TR-Nets($r = 15$) ^{<i>ri</i>}	32.73	0.216	$2.2 \times$
PSTRN-S(Ours)	31.95	0.200	$2.4 \times$

Experimental Results The results for ResNet20 and ResNet32 are given in Table 2 and Table 3. In the Tables 2 and 3, original ResNet20/32 are the model proposed in He et al. (2016). Tucker (Kim et al. 2016) and TT (Garipov et al. 2016) are works that compress neural networks by other tensor decomposition methods. TR-RL (Cheng et al. 2020) search the rank of TR-based model based on reinforcement learning. The first block compares PSTRN-M with the results of low rank decomposition works that have fewer parameters. Obviously, PSTRN-M surpasses other methods in both classification accuracy and compression ratio. The second block reports the performance of PSTRN-S and models that are poor on compression. Results tell that our algorithm achieve high performance and beyonds works with 0.10+M parameters.

In addition, through transferring the searched PSTRN-M/S on CIFAR10 into CIFAR100, PSTRN obtain excellent results as well. This proves that our proposed PSTRN can not only find well-performed models, but also possesses transferability .

4.4 Experiments on HMDB51

The HMDB51 dataset is a large collection of realistic videos from various sources, such as movies and web videos. The dataset is composed of 6766 video clips from 51 action categories.

Experimental Setting In this experiment, we sample 12 frames from each video clip randomly. And then we extract features from the frames via Inception-V3 (Szegedy et al. 2016) input vectors and reshape it into 64×32 . The shape of hidden layer tensor is set as $32 \times 64 = 2048$. For TR-

LSTM, the rank is denoted as $\mathbf{R} = \{R_0, R_1, R_2, R_3 | R_* \in \{15, 16, \dots, 60\}\}$. The complexity of enumerating approach is $46^4 \approx 4.5 \times 10^6$, while the computational complexity of our PSTRN is $n_{gen} \times pop_size \times P = 20 \times 20 \times 3 = 1200$ that is much smaller.

Experimental Results The comparison between our approach and manually-designed method is shown in Table 4. Experimental results show that our searched rank exceed in others with equal rank elements.

Remark Unlike the Pytorch, Keras is a high level package with many tricks under the table, e.g. hard sigmoid in RNNs. Thus, for fairer comparison and validation of search results, we implement this experiment in Pytorch and remove the tricks in the Keras package. Additionally, through Keras implement, our searched TR-LSTM achieve 64.5% accuracy with a compression ratio 48 , which is better than 63.8% with a compression ratio 25 (Pan et al. 2019).

Table 4: Results of TR decomposition for LSTM on HMDB51.

Model	Acc(%)	Params(M)	CR
Original	48.15	33.67	1
TR-LSTM($r = 15$) ^{<i>ri</i>}	54.06	16.96	$258.9 \times$
TR-LSTM($r = 30$) ^{<i>ri</i>}	58.35	17.16	$64.7 \times$
TR-LSTM($r = 50$) ^{<i>ri</i>}	57.75	17.62	$23.3 \times$
TR-LSTM($r = 60$) ^{<i>ri</i>}	58.05	17.93	$16.2 \times$
PSTRN-M(Ours)	59.67	17.26	$46.7 \times$
PSTRN-S(Ours)	60.04	17.38	$34.7 \times$

5 Discussion

Another important component is the shape of a tensor ring decomposition. The method of choosing the shape is notorious. And actually there are almost not any way to select the shape efficiently. Therefore, our PSTRN simply chooses a shape with a similar size by manipulation. The effect of shape on TR-based model is unknown and waits be solved in the future.

Generally, the rank has similar attribution in different kinds of tensor decomposition like Tucker, Tensor Train and so on. It is reasonable to assume that the Hypothesis 1 is suitable for them. Therefore, it is promising to employ PSTRN on them to explore their potential power.

6 Conclusion

In this paper, we design a novel algorithm PSTRN based on Hypothesis 1 to search optimal rank. As a result, our algorithm compress LeNet-5 with $16 \times$ compression ratio and 0.22% accuracy improvement on MNIST. And on CIFAR10 and CIFAR100, our work achieve state-of-the-art performance with a high compression ratio for ResNet20 and ResNet32. Not only the CNN, we also shows excellent performance of RNN on HMDB51. Further, for large-scale datasets, we will explore more performance evaluation acceleration strategies to optimize rank elements more efficiently.

References

- Chen, Y.; Zhao, D.; Lv, L.; and Zhang, Q. 2018. Multi-task learning for dangerous object detection in autonomous driving. *Inf. Sci.* 432: 559–571.
- Cheng, Z.; Li, B.; Fan, Y.; and Bao, Y. 2020. A Novel Rank Selection Scheme in Tensor Ring Decomposition Based on Reinforcement Learning for Deep Neural Networks. In *2020 IEEE International Conference on Acoustics, Speech and Signal Processing, ICASSP 2020, Barcelona, Spain, May 4–8, 2020*, 3292–3296. IEEE.
- Deb, K.; Agrawal, S.; Pratap, A.; and Meyarivan, T. 2002. A fast and elitist multiobjective genetic algorithm: NSGA-II. *IEEE Trans. Evol. Comput.* 6(2): 182–197.
- Deng, L. 2012. The MNIST Database of Handwritten Digit Images for Machine Learning Research [Best of the Web]. *IEEE Signal Process. Mag.* 29(6): 141–142.
- Garipov, T.; Podoprikin, D.; Novikov, A.; and Vetrov, D. P. 2016. Ultimate tensorization: compressing convolutional and FC layers alike. *CoRR* abs/1611.03214.
- He, K.; Zhang, X.; Ren, S.; and Sun, J. 2016. Deep Residual Learning for Image Recognition. In *2016 IEEE Conference on Computer Vision and Pattern Recognition, CVPR 2016*, 770–778. IEEE Computer Society.
- Kim, Y.; Park, E.; Yoo, S.; Choi, T.; Yang, L.; and Shin, D. 2016. Compression of Deep Convolutional Neural Networks for Fast and Low Power Mobile Applications. In *4th International Conference on Learning Representations, ICLR 2016*.
- Kingma, D. P.; and Ba, J. 2015. Adam: A Method for Stochastic Optimization. In *3rd International Conference on Learning Representations, ICLR 2015, San Diego, CA, USA, May 7–9, 2015, Conference Track Proceedings*.
- Krizhevsky, A.; Hinton, G.; et al. 2009. Learning multiple layers of features from tiny images .
- Kuehne, H.; Jhuang, H.; Garrote, E.; Poggio, T. A.; and Serre, T. 2011. HMDB: A large video database for human motion recognition. In *IEEE International Conference on Computer Vision, ICCV 2011, Barcelona, Spain, November 6–13, 2011*, 2556–2563. IEEE Computer Society.
- Lane, N. D.; Bhattacharya, S.; Georgiev, P.; Forlivesi, C.; and Kawsar, F. 2015. An Early Resource Characterization of Deep Learning on Wearables, Smartphones and Internet-of-Things Devices. In *Proceedings of the 2015 International Workshop on Internet of Things towards Applications, IoT-App 2015*, 7–12. ACM.
- LeCun, Y.; Bottou, L.; Bengio, Y.; and Haffner, P. 1998. Gradient-based learning applied to document recognition. *Proceedings of the IEEE* 86(11): 2278–2324.
- Li, D.; Zhao, D.; Chen, Y.; and Zhang, Q. 2018. DeepSign: Deep Learning based Traffic Sign Recognition. In *2018 International Joint Conference on Neural Networks, IJCNN 2018*, 1–6. IEEE.
- Li, W.; Zhu, Y.; Zhao, D.; et al. 2019. Multi-Agent Reinforcement Learning Based on Clustering in Two-Player Games. In *IEEE Symposium Series on Computational Intelligence, SSCI 2019, Xiamen, China, December 6–9, 2019*, 57–63. IEEE.
- Pan, Y.; Xu, J.; Wang, M.; Ye, J.; Wang, F.; Bai, K.; and Xu, Z. 2019. Compressing Recurrent Neural Networks with Tensor Ring for Action Recognition. In *The Thirty-Third AAAI Conference on Artificial Intelligence, AAAI 2019, Honolulu, Hawaii, USA, January 27 - February 1, 2019*, 4683–4690. AAAI Press.
- Real, E.; Moore, S.; Selle, A.; Saxena, S.; Suematsu, Y. L.; Tan, J.; Le, Q. V.; and Kurakin, A. 2017. Large-Scale Evolution of Image Classifiers. In *Proceedings of the 34th International Conference on Machine Learning, ICML 2017, Sydney, NSW, Australia, 6–11 August 2017*, volume 70 of *Proceedings of Machine Learning Research*, 2902–2911. PMLR.
- Ruder, S. 2016. An overview of gradient descent optimization algorithms. *CoRR* abs/1609.04747. URL <http://arxiv.org/abs/1609.04747>.
- Shao, K.; Zhao, D.; Li, N.; and Zhu, Y. 2018. Learning Battles in ViZDoom via Deep Reinforcement Learning. In *2018 IEEE Conference on Computational Intelligence and Games, CIG 2018*, 1–4. IEEE.
- Simonyan, K.; and Zisserman, A. 2015. Very Deep Convolutional Networks for Large-Scale Image Recognition. In *3rd International Conference on Learning Representations, ICLR 2015*.
- Szegedy, C.; Vanhoucke, V.; Ioffe, S.; Shlens, J.; and Wojna, Z. 2016. Rethinking the Inception Architecture for Computer Vision. In *2016 IEEE Conference on Computer Vision and Pattern Recognition, CVPR 2016, Las Vegas, NV, USA, June 27–30, 2016*, 2818–2826. IEEE Computer Society.
- Wang, J.; Bai, H.; Wu, J.; and Cheng, J. 2020. Bayesian Automatic Model Compression. *IEEE Journal of Selected Topics in Signal Processing* .
- Wang, W.; Sun, Y.; Eriksson, B.; Wang, W.; and Aggarwal, V. 2018. Wide Compression: Tensor Ring Nets. In *2018 IEEE Conference on Computer Vision and Pattern Recognition, CVPR 2018*, 9329–9338. IEEE Computer Society.
- Xiao, H.; Rasul, K.; and Vollgraf, R. 2017. Fashion-MNIST: a Novel Image Dataset for Benchmarking Machine Learning Algorithms. *CoRR* abs/1708.07747.
- Yerlan, I.; and Miguel, Á. C. 2020. Low-Rank Compression of Neural Nets: Learning the Rank of Each Layer. In *2020 IEEE/CVF Conference on Computer Vision and Pattern Recognition, CVPR 2020, Seattle, WA, USA, June 13–19, 2020*, 8046–8056. IEEE.
- Zhao, D.; Chen, Y.; Lv, L.; et al. 2017. Deep Reinforcement Learning With Visual Attention for Vehicle Classification. *IEEE Trans. Cogn. Dev. Syst.* 9(4): 356–367.
- Zoph, B.; and Le, Q. V. 2017. Neural Architecture Search with Reinforcement Learning. In *5th International Conference on Learning Representations, ICLR 2017, Toulon, France, April 24–26, 2017, Conference Track Proceedings*. OpenReview.net.

A Supplementary Material

A.1 Tensor Background

In this part, we would like to introduce the background of tensor.

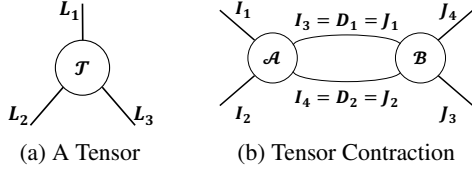


Figure 8: Tensor diagrams. (a) presents the graphical notation of a tensor $\mathcal{T} \in \mathbb{R}^{L_1 \times L_2 \times L_3}$. (b) demonstrates the contraction between two 4-order tensors, which is the contraction between \mathcal{A} and \mathcal{B} .

Notation A tensor is a high-order array. In this paper, a d -order tensor $\mathcal{T} \in \mathbb{R}^{L_1 \times L_2 \times \dots \times L_d}$ is denoted by a boldface Euler script letter. With all subscripts fixed, each element of a tensor is expressed as: $\mathcal{T}_{l_1, l_2, \dots, l_d} \in \mathbb{R}$. Given a subset of subscripts, we can get a sub-tensor. For example, given a subset $\{L_1 = l_1, L_2 = l_2\}$, we can obtain a sub-tensor $\mathcal{T}_{l_1, l_2} \in \mathbb{R}^{L_3 \times \dots \times L_d}$. Figure 8 draws the tensor diagrams that present the graphical notations and the essential operations.

Tensor Contraction Tensor contraction can be performed between two tensors if some of their dimensions are matched. As shown in Figure 8b, given two 4-order tensors $\mathcal{A} \in \mathbb{R}^{I_1 \times I_2 \times I_3 \times I_4}$ and $\mathcal{B} \in \mathbb{R}^{J_1 \times J_2 \times J_3 \times J_4}$, when $I_3 = D_1 = J_1$ and $I_4 = D_2 = J_2$, the contraction between these two tensors results in a tensor with the size of $I_1 \times I_2 \times J_3 \times J_4$, where the matching dimension is reduced, as shown in Equation (15):

$$(\mathcal{AB})_{i_1, i_2, j_3, j_4} = \sum_{m=1}^{D_1} \sum_{n=1}^{D_2} \mathcal{A}_{i_1, i_2, m, n} \mathcal{B}_{m, n, j_3, j_4}. \quad (15)$$

Tensorization Given a matrix $\mathbf{M} \in \mathbb{R}^{I \times O}$, we transfer it into a new tensor $\mathcal{C} \in \mathbb{R}^{I_0 \times I_1 \times \dots \times I_{M-1} \times O_0 \times O_1 \times \dots \times O_{N-1}}$, satisfying the equation:

$$\prod_{i=1}^M I_i = I, \quad \prod_{j=1}^N O_j = O,$$

where M, N are the number of the input nodes and output nodes respectively. Therefore, a corresponding element of $\mathbf{W}_{i,o}$ is $\mathcal{C}_{i_0, \dots, i_{M-1}, o_0, \dots, o_{N-1}}$, where $i \in \{1, \dots, I\}$, $o \in \{1, \dots, O\}$, $i_* \in \{1, \dots, I_*\}$, $o_* \in \{1, \dots, O_*\}$ are indexes, following the rule *

$$i = \sum_{u=1}^M \prod_{v=1}^{i_u-1} I_v(i_u - 1), \quad o = \sum_{u=1}^N \prod_{v=1}^{o_u-1} O_v(o_u - 1). \quad (16)$$

*Here, define $\prod_v^0(\bullet) = 1, v > 0$.

A.2 Pseudocode for PSTRN

In this section, we depict the algorithm of PSTRN as below, where P is the number of progressive phase, and G is the generations of each evolutionary phase.

Algorithm 1 Progressive Searching Tensor Ring Network

Input: Datasets \mathcal{D} , generations of evolutionary phase \mathcal{G} , number of progressive phase \mathcal{P} .
Initialize the search space
for $p = 1, 2, \dots, P$ **do**
 if Large-scale model (TR-ResNets) **then**
 Do warm-up of weights
 end if
 Generate a set of randomized ranks
 Compute their accuracy and compression ratios via
 for $g = 1, 2, \dots, G$ **do**
 Do selection, mutation and crossover
 Obtain the promising rank
 end for
 Determine the search space for next phase
end for
Output: A set of well-performed tensor ring rank elements

A.3 Experimental Setups and Results

TR-LeNet-5 on MNIST and Fashion MNIST We search for TR-LeNet-5 on MNIST (Deng 2012) and Fashion MNIST (Xiao, Rasul, and Vollgraf 2017) (10 classes, 60k grayscale images of 28×28).

Table 5: Results on Fashion MNIST.

Model	Error(%)	Params(K)	CR
Original ^{ri}	7.4	429	1
TR-Nets($r = 10$) ^{ri}	9.63	16	$26.5 \times$
TR-Nets($r = 20$) ^{ri}	8.67	65	$6.6 \times$
TR-Nets($r = 30$) ^{ri}	8.64	145	$3.0 \times$
PSTRN-M(Ours)	8.05	49	$8.8 \times$
PSTRN-S(Ours)	7.85	62	$6.9 \times$

TR-LeNet-5 is trained by Adam (Kingma and Ba 2015) on mini-batches of size 128. The random seed is set to 233. The loss function is cross entropy. Models are trained for 20 epochs with an initial learning rate as 0.002 that is decreased by 0.9 every 5 epochs. PSTRN runs 40 generations at each evolutionary phase with population size 30. The number of rank elements searched is 20. The number of progressive phase is 3. The interval b_* of each phase is 5, 2 and 1 respectively.

Experimental results of TR-LeNet-5 on Fashion MNIST is demonstrated in Table 5. TR-Nets (Wang et al. 2018) are the special cases of TR-LeNet5, whose rank elements are all equal to r . The superscript ri represents a re-implement model. Obviously, our PSTRN can exceed models that set rank manually. In addition, as shown in Figure 9, our approach can also achieve best performance compared with

Table 6: Rank of searched TR-LeNet-5.

Model	Error(%)	Rank
MNIST		
PSTRN-M	0.57	{6,20,14,8,12,20,2,20,16,16,20,12,12,8,6,26,8,2,6,20}
PSTRN-S	0.49	{2,24,18,8,8,30,18,30,22,26,22,26,30,14,30,8,24,12,10,30}
Fashion MNIST		
PSTRN-M	8.05	{8,14,8,18,14,18,22,28,6,24,20,14,20,20,10,22,20,20,6,20}
PSTRN-S	7.85	{22,12,6,22,16,22,30,22,16,18,24,30,30,8,30,24,22,20,6,18}

manually setting models on MNIST. The ranks of searched TR-LeNet-5 are shown in Table 6.

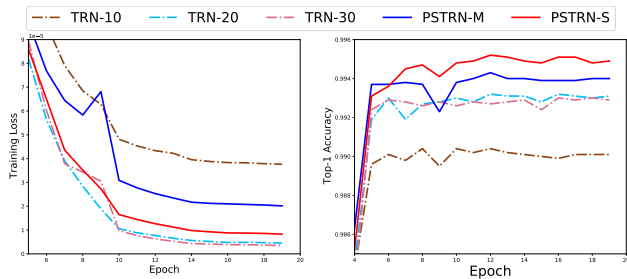


Figure 9: Training process on MNIST. TRN-10/20/30 are TR-Nets that set rank to 10, 20 and 30 respectively. TRN-20 and TRN-30 are over-fitting.

TR-ResNets on CIFAR10 and CIFAR100 We search TR-ResNets on CIFAR10 (10 classes, 60k RGB images of 32×32) and transfer the searched model to CIFAR100 (Krizhevsky, Hinton et al. 2009) (100 classes, 60k RGB images of 32×32).

TR-ResNets are trained via SGD (Ruder 2016) with momentum 0.9 and a weight decay of 5×10^{-4} on mini-batches of size 128. The random seed is set to 233. The loss function is cross entropy. TR-ResNets are trained for 200 epochs with an initial learning rate as 0.02 that is decreased by 0.8 after every 60 epochs. Our approach runs 20 generations at each evolutionary phase with population size 30. The number of rank elements searched is 7. The number of progressive phase is 3. The interval b_* of each phase is 3, 2 and 1 respectively.

The ranks of searched TR-ResNet20 and TR-ResNet32 are shown in Table 7 and 8.

TR-LSTM on HMDB51 We search TR-LSTM on HMDB51 (Kuehne et al. 2011) (51 classes, 6766 video clips).

TR-LSTM is trained via Adam with a weight decay of 1.7×10^{-4} on mini-batches of size 32. The random seed is set to 233. The loss function is the cross entropy. In search

Table 7: Rank of searched TR-ResNet20.

Model	Error(%)	Rank
CIFAR10		
PSTRN-M	11.5	{ 4, 8, 6, 8, 6, 12, 10 }
PSTRN-S	9.2	{ 8, 15, 10, 12, 14, 18, 12 }
CIFAR100		
PSTRN-M	36.38	{ 8, 10, 6, 8, 8, 12, 12 }
PSTRN-S	33.87	{ 8, 15, 10, 12, 14, 18, 12 }

Table 8: Rank of searched TR-ResNet32.

Model	Error(%)	Rank
CIFAR10		
PSTRN-M	9.4	{ 3, 12, 9, 9, 9, 9, 6 }
PSTRN-S	8.56	{ 17, 14, 10, 13, 18, 15, 10 }
CIFAR100		
PSTRN-M	33.23	{ 4, 8, 6, 8, 12, 12, 10 }
PSTRN-S	31.95	{ 16, 14, 12, 14, 20, 16, 8 }

phase, searched models are trained for 100 epochs with an initial learning rate as $1e-5$. Our approach runs 20 generations at each evolutionary phase with population size 20. The number of rank elements searched is 4. The number of progressive phase is 3. The interval b_* of each phase is 8, 3 and 1 respectively.

Table 9 demonstrates the ranks for TR-LSTM that searched via PSTRN.

Table 9: Rank of searched TR-LSTM.

Model	Acc(%)	Rank
PSTRN-M	59.67	{ 52, 17, 34, 37 }
PSTRN-S	60.04	{ 45, 42, 36, 42 }